Journal of Theoretical Biology 313 (2012) 68–78

Contents lists available at SciVerse ScienceDirect

Journal of Theoretical Biology

journal homepage: www.elsevier.com/locate/yjtbi

Elastic recoil can either amplify or attenuate muscle–tendon power, depending on inertial vs. fluid dynamic loading

Christopher T. Richards [a,*], Gregory S. Sawicki [b]

[a] The Rowland Institute at Harvard, Harvard University, 100 Edwin H. Land Blvd, Cambridge, MA 02142, USA
[b] Department of Biomedical Engineering, North Carolina State University & University of North Carolina at Chapel Hill, 911 Oval Drive, Campus Box 7115, NC State University, Raleigh, NC 27695-7115, USA

HIGHLIGHTS

- We model a muscle–tendon to explore environment-morphology effects on power output.
- Models predict that power amplification occurs with both inertial and fluid loading.
- Elastic energy storage does not necessarily benefit locomotor performance.
- Inertial vs. fluid-dynamic loading governs the timing of elastic recoil.

ARTICLE INFO

Article history:
Received 27 January 2012
Received in revised form
25 July 2012
Accepted 31 July 2012
Available online 8 August 2012

Keywords:
Muscle power amplification
Gearing
Mechanical advantage
Mathematical model
Inertial and viscous loads

ABSTRACT

Frog jumps exceed muscle power limits. To achieve this, a muscle may store elastic energy in tendon before it is released rapidly, producing 'power amplification' as tendon recoil assists the muscle to accelerate the load. Do the musculoskeletal modifications conferring power amplification help or hinder frog swimming? We used a Hill-type mathematical model of a muscle–tendon (MT) with contractile element (CE) and series elastic element (SEE) properties of frogs. We varied limb masses from 0.3 to 30 g, foot-fin areas from 0.005 to 50 cm^2 and effective mechanical advantage (*EMA*=in-lever/out-lever) from 0.025 to 0.1. 'Optimal' conditions produced power amplification of ~19% greater than the CE limit. Yet, other conditions caused ~80% reduction of MT power (power attenuation) due to SEE recoil absorbing power from (rather than adding to) the CE. The tendency for elastic recoil to cause power amplification vs. attenuation was load dependent: low fluid drag loads, high limb mass and *EMA*=0.1 caused power amplification whereas high drag, low mass and low *EMA* (=0.025) caused attenuation. Power amplification emerged when: (1) CE shortening velocity is $1/3V_{max}$, (2) elastic energy storage is neither too high nor too low, and (3). peak inertial-drag force ratio $\geq$ ~1.5. Excessive elastic energy storage delayed the timing of recoil, causing power attenuation. Thus our model predicts that for fluid loads, the benefit from a compliant tendon is modest, and when the system is 'poorly tuned' (i.e., inappropriate *EMA*), MT power attenuation can be severe.

1. Introduction

Both in swimming and in jumping, frogs achieve astonishing accelerations. Their great jumping ability is born in part from unique traits of the skeleton (Emerson, 1978; Shubin and Jenkins 1994;Reilly and Jorgensen, 2011) and musculature (Lutz and Rome, 1994; Azizi and Roberts, 2010). Yet, despite impressive power outputs from *in vitro* muscle (James and Wilson, 2008), the power exerted on the frog body far exceeds theoretical muscle power output (Marsh and John-Alder, 1994; Peplowski and Marsh, 1997). As hinted by Emerson (Emerson, 1978) and supported by later studies (Marsh and John-Alder 1994; Peplowski and Marsh, 1997; Astley and Roberts, 2011), the additional power likely emerges as muscles contract to stretch spring-like tendons, then quickly release the energy to drive the legs. Since energy is stored slowly compared to energy release, there is an apparent 'power amplification' as the power output of the recoiling spring exceeds the muscle power input to pre-stretch the spring. Such behavior requires particular properties of morphology (e.g., tendon stiffness) and physiology (e.g., muscle contraction speed; Galantis and Woledge, 2003; Roberts and Marsh, 2003). However, since the consequences of such specializations on swimming performance are unknown, we ask: does tendon elastic recoil enhance or hinder swimming ability in frogs?

* Corresponding author. Tel.: +1 617 497 4683.
E-mail address: richards@fas.harvard.edu (C.T. Richards).

0022-5193/$ - see front matter © 2012 Elsevier Ltd. All rights reserved.
http://dx.doi.org/10.1016/j.jtbi.2012.07.033

Independent of locomotor environment, the need for power amplification arises from the force-velocity relationship of muscle. Since the available force from muscles decays steeply with shortening velocity (Hill, 1938), muscle power follows a bell-shaped pattern. This power-velocity curve therefore reveals a power limit occurring at $\sim 1/3$ maximum shortening velocity (V_{max}). Although a muscle may generate maximum power output against a load by operating near $\sim 1/3V_{max}$ (Rome et al., 1988; Lutz and Rome, 1994), tasks requiring additional instantaneous power must rely on the recoil of elastic structures (tendon, aponeurosis, etc.) arranged in-series with muscle fibers. For example, a catch mechanism (Bennet-Clark and Lucey, 1967) can enable the muscle to load the tendon prior to load movement. Subsequently, recoil occurs ballistically after catch release. Alternatively, power amplification can arise against an unrestrained load when the instantaneous muscle power is enhanced by the addition of power from the recoiling tendon. Since there is no evidence of a catch mechanism in swimming frogs, we focus on the latter mechanism.

Despite energy-saving mechanisms in cyclic motion (Alexander, 1997) and power amplification in maximal burst performance (Roberts and Marsh, 2003), elastic recoil does not always confer mechanical benefits. To illustrate this point, we discuss a simple muscle–tendon (MT) where a muscle contractile element (CE) connects through a series elastic element (SEE; e.g., tendon) to pull a mass (Fig. 1A). Depending on the mass, the MT operates between two extremes known as 'isometric' (fixed-end) contraction and unloaded contraction. If the mass is large, active fibers can shorten to store energy internally within in-series elastic tissues, rather than moving the load. Conversely when the load is nearly massless, the MT shortening velocity approaches V_{max} at minimum CE force. Neither of the above cases produce power on the load. Instead, for power output to occur, the MT must operate between either extreme, as outlined in three hypothetical cases: (1) power transmitting, (2) power attenuating and (3) power enhancing. (1) In a power transmitting example, the external load is too small to cause significant storage of elastic energy. Nearly all of the muscle mechanical power is transmitted directly to the load (CE power $\approx$ load power). (2) At the other extreme, if the mass is large, the muscle generates power to stretch the tendon. Since the large mass resists acceleration, the subsequent release of stored energy 'backfires' as the muscle begins to relax, lengthening the CE rather than moving the load. Such was observed during submaximal frog jumps (Astley and Roberts, 2011). Since elastic backfire reduces muscle velocity, the power exerted against the load is attenuated by in-series elasticity (CE power > load power). (3) Power enhancement, in contrast, occurs at intermediate loads. Unlike elastic backfire, elastic energy stored initially enables the SEE to recoil to move the load, rather than pulling and lengthening the CE. Consequently, the power exerted against the load is greater than CE power alone (CE power < load power). Hence, 'power amplification' (e.g., Gray and Mill, 1983; Aerts, 1998) is a special case of power enhancement where the CE reaches maximum (or near maximum) power output, shortening at $\sim 1/3V_{max}$, while the additional power from elastic recoil produces MT power exceeding the theoretical limits for muscle alone. In the current study, we explore the tuning of morphological parameters to 'optimize' MT power output under various external loading conditions.

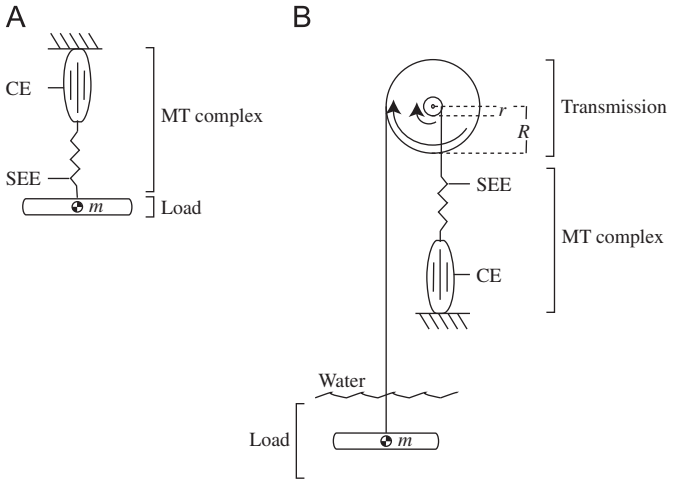

Fig. 1. Schematic diagrams illustrate a muscle–tendon (MT) complex comprised of a contractile element (CE) with Hill-type force-velocity properties and an elastic element (SEE) for (A) a simple inertial load coupled directly to the MT and (B) an inertial and fluid drag-based load coupled to the MT via a transmission. As the MT rotates the smaller pulley, the larger pulley rotates at the same angular velocity to move the mass. The inlever radius (r) and outlever radius (R) of the two pulleys determine the effective mechanical advantage ($EMA = r/R$) of the MT on the load. Gravitational force was not considered in either case.

For purely inertial or inertial+gravitational loads (e.g., during jumping) both the effective mechanical advantage (EMA=in lever/out lever) and the load's mass are the key parameters determining MT power output. For example, since load force depends on EMA (load force = MT force $\times$ EMA), a decrease in EMA causes an increase in MT force and elastic energy storage for a given load. Consequently if load force is small, the EMA must also be small to maintain the same MT power output.

Given the importance of EMA and mass on power output, semi-aquatic frogs that must move effectively both on land and in water might be subject to additional constraints. Particularly, swimming frogs exert lower forces against fluid than during jumping on land (Nauwelaerts and Aerts, 2003; Nauwelaerts et al., 2005), suggesting that the 'optimal' parameters for swimming might be different from jumping. For example, jumping bullfrogs require an EMA of ~ 0.12 to maximize the contribution of elastic recoil (Roberts and Marsh, 2003). However, for $EMA = 0.12$, MT power falls steeply as load decreases (Galantis and Woledge, 2003), suggesting that frogs must decrease their EMA to compensate for lower load forces during swimming. Thus we hypothesize that the morphological conditions which maximize MT power for inertial loads are sub-optimal for fluid loads characteristic of swimming (and vice versa). Specifically, we expect that EMA must be lowered to increase the effective load to maximize the contribution of elastic recoil to MT power against fluid loads.

We implemented a mathematical simulation using physiological and morphological parameters based on the plantaris longus (PL) muscle–tendon from swimming frogs (i.e., *Xenopus laevis*). As used in prior work (Galantis and Woledge, 2003) the model is an 'idealized' muscle consisting of a Hill-type force-velocity actuator in series with a 'Hookean' spring. As in the Galantis and Woledge model, the muscle was assumed to contain infinite sarcomeres such that the muscle may shorten indefinitely without experiencing length-tension effects. Additionally, our model consists of a MT complex which translates a flat plate through water via a massless set of pulleys to simulate limb transmission EMA (Fig. 1B). Given the intrinsic MT properties (e.g., V_{max}, F_{max}, and SEE stiffness, k) we simulated trials over a range of EMA values. Since power amplification is likely most relevant for a single burst of escape (i.e., maximal) performance, we used identical maximal stimulation conditions for all of the simulations. Additionally, to address the relative influences of inertial vs. drag loading, the plate's mass and fluid dynamic coefficients were varied.

2. Materials and methods

2.1. Formulation of the muscle–tendon model

To obtain the equation of motion for the system we applied linear momentum balance (i.e., Newton's 2nd Law) to a rectangular

plate, including inertial and viscous loading as described in Fig. 1B to yield Eq. (1):

$$\overbrace{F_{out\text{-}load}}^{MT\times EMA} - \overbrace{F_{drag}}^{DRAG} = \overbrace{m\frac{d^2x_{load}}{dt^2}}^{INERTIAL} \tag{1}$$

where $F_{out\text{-}load}$ is the force exerted on the load from the output side of the transmission, F_{drag} is the reaction force on the load due to viscous drag effects of the fluid medium, m is the mass of the load (i.e., a rectangular plate representing a *Xenopus* foot) and x_{load} is the vertical position of the load relative to the pulley center of rotation (see Fig. 1B).

We assumed a velocity-dependent drag force (Eq. (2)):

$$F_{drag} = \beta \times \left(\frac{dx_{load}}{dt}\right)^2 \tag{2}$$

with a drag multiplier, β (Eq. (3)):

$$\beta = \frac{1}{2} C_d \rho A_{plate} \tag{3}$$

where $C_d \approx 1$ for a rectangular plate (Hoerner, 1965), ρ is the fluid viscosity (i.e., 1000 kg/m^3 for water) and A_{plate} is the cross sectional area of a rectangular 'foot'. We did not explicitly include fluid added mass in our model. Fluid added mass coefficients for translational motion are often modeled as constants based on foot geometry (e.g., Aerts and Nauwelaerts, 2009). In our case, representing added mass separately would not change the behavior of the model. Rather, it would only shift the mass values by a small offset (negligible compared to our values which differ by orders of magnitude). Therefore, the 'mass' term in our model represents the virtual mass (added mass+foot mass). Next, assuming a massless pulley transmits the muscle–tendon (MT) force to the load, and applying angular momentum balance about the pulley center of rotation yields Eq. (4):

$$F_{out\text{-}load} = \left(\frac{r}{R}\right) \times F_{in\text{-}mt} \tag{4}$$

where r is the moment arm of the MT force on the input side of the pulley (i.e., inlever), $F_{in\text{-}mt}$, R is the moment arm of the load on the output side of the pulley (i.e., outlever) and r/R is the effective mechanical advantage ($EMA=r/R$) of the transmission.

The in-lever force generated by the MT is developed by a contractile element (CE) with an elastic element (i.e., tendon and aponeurosis) in series (SEE), yielding Eq. (5):

$$F_{in\text{-}mt} = F_{see} = F_{ce} \tag{5}$$

We modeled the CE force output as a classical Hill-type muscle actuator with first-order activation dynamics and non-linear force-velocity properties (Zajac, 1989) (Eq. (6)):

$$F_{ce} = F_{\max} \times f(act_{ce}) \times f(v_{ce}) \tag{6}$$

with the maximum isometric muscle force $F_{\max}=10$ N based on *in vivo* data from *Xenopus laevus* (Richards and Biewener, 2007). Additionally, from measurements of muscle physiological cross sectional area of $\sim$0.5 cm^2 and rest length=2 cm (Richards, 2011), the muscle was modeled as a cylinder with a density of 1.06 g/cm^3 and therefore a mass of 0.00106 kg. Hence, for the current study, all power values are reported in mW ($\approx$W/kg-muscle). Initial pilot simulations also included a force-length component in Eq. (6), but this only served to attenuate the absolute values of force and mechanical power without altering the observed trends in the morphology-environment parameter space under study. Therefore, for simplicity, none of the simulations presented here incorporate force-length effects (see Discussion for further details).

Excitation-activation coupling was governed by a simple first-order differential equation (Eq. (7)):

$$f(act_{ce}) \rightarrow a \times \frac{dact_{ce}}{dt} + b \times act_{ce} = u(t) \tag{7}$$

with constants $a=0.0625$ and $b=0.625$ set so that a step input excitation (i.e., $u(t)=1.0$) resulted in full-activation (i.e., $a(t)=1.0$) after 100 ms, resulting in time-to-peak tension ($\sim$120 ms) similar to that observed in vivo in swimming frogs (Richards and Biewener, 2007) and in vitro in *Xenopus laevus* plantaris tetanic contractions (Richards, unpublished observations).

We modeled force-velocity dynamics following standard equations for shortening (Eq. (8a)) and lengthening (Eq. (8b)) contractions (Otten, 1987; Hill, 1938):

$$f(v_{ce}) = \frac{(1 - V_{ce}/V_{\max})}{[1 + V_{ce}/(0.25 \times V_{\max})]} \quad \text{for} \quad V_{ce} \geq 0 \text{ (i.e., shortening)} \tag{8a}$$

$$f(v_{ce}) = 1.8 - \frac{0.8 \times (1 + V_{ce}/V_{\max})}{[1 - 7.56 \times V_{ce}/(0.25 \times V_{\max})]} \quad \text{for} \quad V_{ce} < 0 \text{ (i.e., lengthening)} \tag{8b}$$

where V_{ce} is the CE shortening velocity (i.e., negated CE velocity) and $V_{\max}$ is the maximum CE shortening velocity. We used $V_{\max}=9$ (i.e., 180 mm/s or $\sim$9 muscle rest lengths/s) which is in the range of observed values for *Xenopus laevis* plantaris muscle. Hence, the maximum CE power output predicted by the force-velocity curve (occurring at $\sim 1/3\ V_{\max}$)=171.9 mW.

Finally, to calculate V_{ce} (i.e., $V_{ce}=dL_{ce}/dt$) we applied the constraint equation (Eq. (9)):

$$\Delta L_{ce} + \Delta L_{see} + \Delta L_{mt} = 0 \tag{9}$$

with SEE length change following from behavior exhibited by a linear Hookean spring (Eq. (9))

$$\Delta L_{see} = \frac{F_{see}}{k} \tag{10}$$

and L_{mt} following from twice integrating Eq. (1) to get x_{load} and then applying Eq. (11):

$$\Delta L_{mt} = \Delta x_{load} \times EMA \tag{11}$$

We used MATLAB/Simulink (Mathworks Inc, Natick, MA) to numerically integrate Eq. (1), applying the relationships described in Eqs. (2)–(11). We could then extract force, length, velocity and mechanical power (i.e., force $\times$ velocity) as functions of time for the load (separated into intertial and drag components) as well as the MT and its components (CE and SEE). Each simulation was a single muscle contraction (i.e., power stroke) initiated by a square wave excitation $u(t)=1$ for 100 ms duration.

A range of stiffness (k) values from 1250 to 5000 N/m were initially tested. These values were based on a nominal value of 2500 N/m estimated by assuming a tendon strain equivalent to 20% muscle strain at force=Po (Roberts and Marsh, 2003). Initial simulation runs, however, only caused small ($\sim$1%) changes in MT power output. Therefore, we selected a constant k value (1250 N/m) which yielded the highest MT power outputs for the current study (see Discussion for further details).

2.2. Parameter study and sensitivity analysis

A parameter study in morphology-environment space was conducted using a factorial approach. Each condition level for each parameter was tested against all other parameter condition levels giving 45 simulation conditions ($3\times5\times3$) for m, β and EMA, respectively. Additionally, a sensitivity analysis was performed for all 45 conditions. Specifically, each parameter value was increased by 10% at each point in the $3\times5\times3$ parameter

space to determine the relative influences of mass, β, and *EMA* on MT power output. Simulations were broadly grouped as power amplifying (peak instantaneous MT power output/CE power limit >1), power attenuating (minimum instantaneous CE power output <0 during elastic recoil), or between the two extremes.

Mass (m) and drag multiplier (β) each were varied by orders of magnitude to encompass a biologically relevant range of values. The middle values for m and β were based on measurements of a 30 g frog, giving a frog and foot mass $=3$ g and a foot area $=5$ cm^2. We used a coefficient of drag for the foot $=1$ (Gal and Blake, 1988) and fluid density $=1000$ g/kg^3 giving $\beta=0.25$ for *X. laevis*. Mass values thus extend from $0.1\times$ actual frog foot mass to 30 g (equivalent to the full frog body mass). Additionally, since three values for β were insufficient for determining the influence of fluid loading, five values were used instead: 2.5×10^{-4}, 2.5×10^{-3}, 2.5×10^{-2}, 2.5×10^{-1} and 2.5. For discussion purposes, we report β in terms of orders of magnitude from 10^{-3} to 10^{1} representing actual β values from 0.00025 to 2.5. Aquatic animals, including frogs, experience a range of drag loading as foot sizes vary. Additionally, variation in β can also represent changes in fluid density (e.g., air vs. water) experienced by a MT system. Finally, *EMA* ($=r/R$) could not be varied by orders of magnitude because large values (>0.5) or small values (<0.02) do not likely occur among vertebrates. The initial *EMA* value was therefore varied from 0.1, similar to the optimal value reported for jumping frogs (Roberts and Marsh, 2003) and for *X. laevis* (Clemente and Richards, 2012). *EMA* was varied from 0.1 to 0.05 to 0.025. Importantly, we did not include the motion of the body in our model. We sought only to determine fundamental properties of muscle–tendon dynamics in fluid in the absence of further complications that might obscure our findings (see Discussion). Therefore, the morphology represented by our parameter set only represents a hypothetical range of muscle–foot properties within which physiological values for frogs lie.

3. Results

3.1. General patterns of force, length and velocity during muscle–tendon simulations

Changes in muscle–tendon (MT) loading conditions dramatically changed muscle–tendon dynamics despite a fixed neural activation-deactivation. Yet, simulation data revealed notable similarities in force, length and velocity patterns across model conditions (Fig. 2). Due to the in-series compliance of the MT model, the pattern of tendon lengthening mirrored the simple shape of MT force for all simulations. The SEE velocity pattern showed initial stretch (negative velocity) followed by shortening (positive velocity). Temporal patterns of contractile element (CE) and MT shortening were more complex and highly sensitive to model parameters. Generally, the MT unit shortened smoothly throughout each simulation. However, as a consequence of tendon compliance, CE shortening velocity often traced multiple peaks before stabilizing after peak MT velocity was reached. In the initial period of muscle activation, shortening of the CE was partially compensated by tendon lengthening. Hence, initial CE velocities often exceeded the shortening rate of the MT unit as the CE stored elastic energy in the tendon. For all simulations, the components of inertial and drag force were out of phase because of the necessary phase lag between acceleration and velocity, respectively. This phase lag has important implications for MT power output (see Discussion for further details).

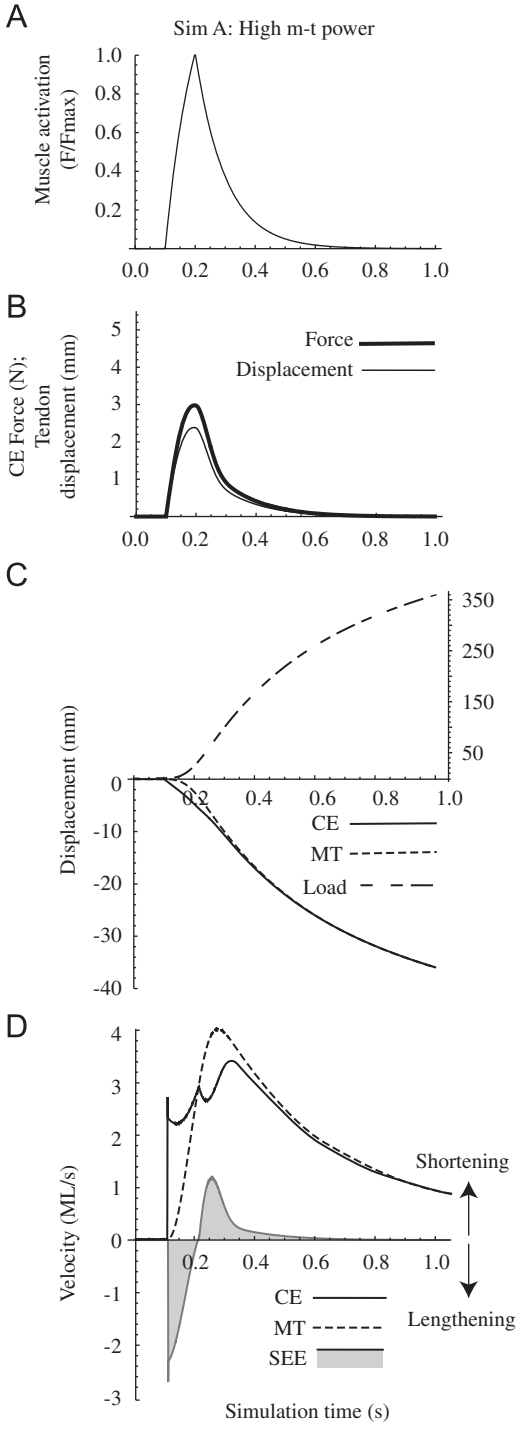

Fig. 2. Raw simulation output showing (A) neural activation-deactivation, (B) contractile element force (CE) and series elastic element (SEE) displacement, (C) CE (solid), muscle–tendon (MT; dashed) and load (short-long dashed) displacement and (D) CE (solid), muscle–tendon (MT; dashed) and SEE (shaded) velocity. Note that shortening velocity is shown as negative. Note also that velocity traces were differentiated from displacement traces.

3.2. The influence of hydrodynamic drag and effective mechanical advantage on muscle–tendon force and power output

As the drag multiplier (β) was increased over five orders of magnitude, peak MT force changed considerably (Fig. 3). Increasing mass, β and gear ratio ($1/EMA$) each caused monotonic increases in peak force. β showed the strongest influence on peak force, particularly for the low mass (0.3 g) simulations which

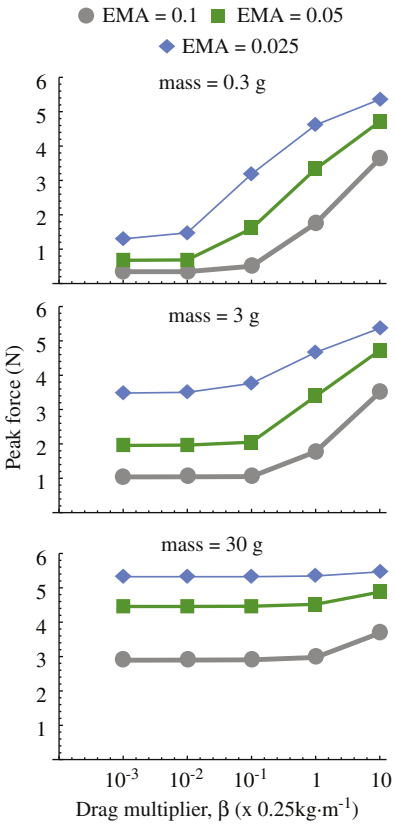

Fig. 3. Peak muscle–tendon (MT) force vs. drag multiplier (β) at *EMA*=0.1 (grey circles), *EMA*=0.05 (green squares) and *EMA*=0.025 (blue diamonds). Upper, middle and lower panels are for mass=0.3 g, 3 g and 30 g simulations. Each point represents a single simulation.

increased more than 300% at each *EMA* level. However, the sensitivity to β decreased with increasing mass such that at high mass (30 g), peak force remained nearly constant. Thus, in the medium and high mass cases, decreases in *EMA* caused greater changes in peak force than β.

Unlike changes in MT force, patterns of power output vs. β were highly dependent upon both the *EMA* and load mass (Fig. 4). Importantly, peak power outputs from the MT, CE and SEE often occurred at different times (see Discussion for further details). Consequently, peak MT power was rarely the sum of peak CE and SEE power outputs. For all of the low mass (0.3 g) cases, maximum power reached ~150 mW, regardless of effective mechanical advantage (*EMA*). Yet, the 'optimal' β for producing MT power shifted from 10^{-2} to 10^{-1} to 1 as *EMA* increased from 0.025 to 0.1 (Fig. 4). This rightward shift in optimal β was not observed in either CE power nor in SEE power. Rather, CE power increased until the maximum CE power limit (~172 mW) with lower *EMA* simulations reaching the plateau at lower β values. Similarly, peak SEE power increased with β more steeply for lower *EMA* values. Unlike CE power output, SEE power trends showed no discernable power limit, although the peak power outputs were lower for the SEE compared to the CE. Similar trends were observed for the mass=3 g simulations, although maximum MT power for each *EMA* decreased from 199 to 167 to 148 mW as *EMA* increased. The lowest *EMA* condition showed the strongest sensitivity to β yielding both the highest and lowest MT power outputs, despite a constant CE power as β increased. Despite similarities in peak power trends for low and intermediate mass cases, the high mass models (30 g) behaved dramatically different. Unlike lower mass models, power outputs from the MT, CE and SEE were all nearly independent of β except for a ~30–50% drop in MT power at β=10. These shifts in peak power trends reported above illustrate important interactions between β, *EMA* and mass conditions which are considered in a sensitivity analysis (see Section 3.5).

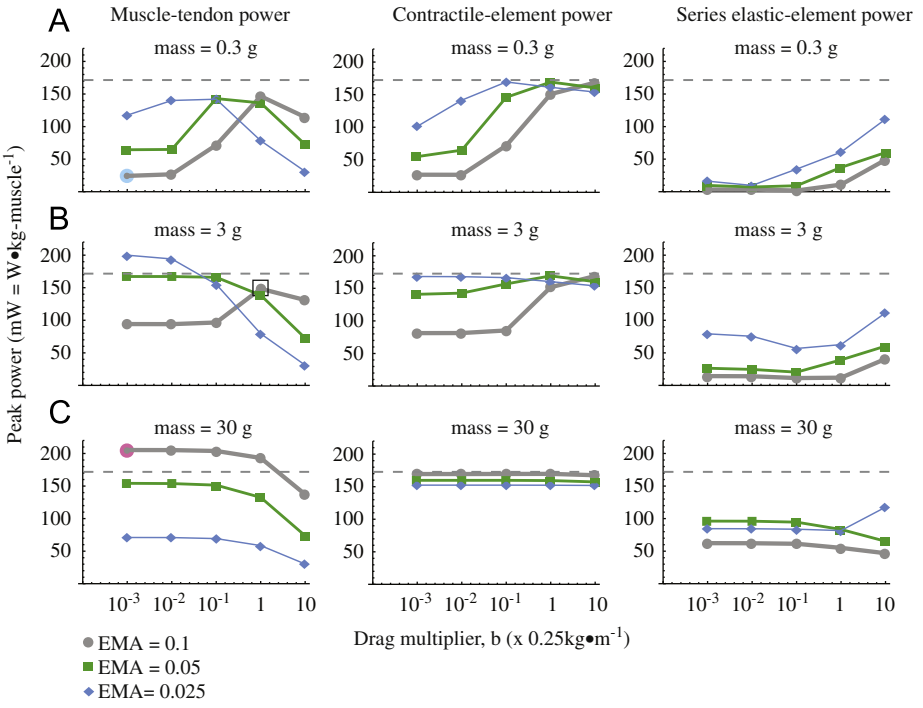

Fig. 4. Components of muscle–tendon (MT) power vs. drag multiplier (β) for (A) mass=0.3 g, (B) mass=3 g and (C) mass=30 g simulations. *EMA*=0.1 (grey circles), *EMA*=0.05 (green squares) and *EMA*=0.025 (blue diamonds). Left, middle and right columns show peak power outputs for the muscle–tendon (MT), contractile element (CE) and elastic element (SEE). Each point represents a single simulation. The lowest MT power output is highlighted by a blue circle, whereas the highest power is highlighted by a red circle. The conditions estimated for *Xenopus laevis* are highlighted by a black box. The dashed grey line represents the CE power limit.

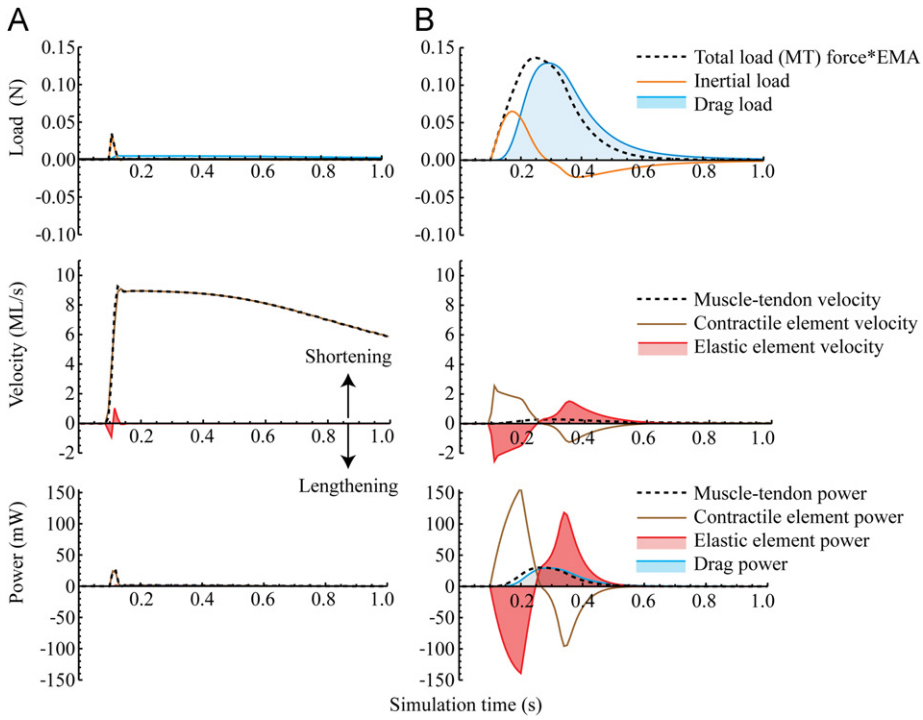

Fig. 5. Data traces from (A) a power transmitting simulation (mass=0.3 g, $\beta=10^{-3}$, *EMA*=0.1) and (B) a power attenuating simulation (mass=30 g, $\beta=10^{1}$, *EMA*=0.025). Upper panels show the total (dashed), inertial (orange) and drag (blue, shaded) components of load. Note that the total load=MT force × *EMA*. Middle panels show muscle–tendon (MT; dashed), contractile element (CE; brown) and series elastic element (SEE; red, shaded) components of velocity. Lower panels show muscle–tendon (MT; dashed), contractile element (CE; brown), drag (blue shaded) and series elastic element (SEE; red, shaded) components of power. Note the phase delay between inertial and drag loads. Also note that panel (A) is the simulation which produced the lowest power in the parameter space.

3.3. Model conditions resulting in poor muscle–tendon power output

Among the loading conditions tested, the simulations producing the lowest MT peak power emerged at opposite extremes of the parameter space. The lowest power output of 25 mW occurred at low mass, high *EMA* (low gear) and low β values (Figs. 4 and 5A). Since both load mass and β were small, there was minimal force output required to accelerate the load. Moreover, high *EMA* further reduced loading by amplifying muscle shortening at the expense of MT force applied to the load. Consequently only −0.16 mJ was stored in the tendon, compared to 1.06 mJ output from the CE. Hence, due to force-velocity effects, the CE accelerated rapidly to ~90% V_{max} causing MT power to decay sharply in the absence of a substantial load. Notably, the highest loading simulation (high mass, high β and low *EMA*) also yielded a low power output of 32 mW (Figs. 4 and 5B). Because of the large external load, the CE stored 12.0 mJ in the SEE (~86% of CE work input). However, the elastic energy release as the muscle deactivated contributed to muscle lengthening (i.e., absorption of muscle power) rather than accelerating the load, resulting in elastic 'backfire' as previously reported in sub-maximal frog jumps (Astley and Roberts, 2011). Furthermore, the timing of elastic recoil did not favor power enhancement because peak SEE recoil power occurred ~100 ms following peak MT power.

3.4. Model conditions resulting in muscle–tendon power enhancement and amplification

Several MT simulation conditions resulted in either power enhancement or amplification. For example, at intermediate mass (3 g), low β and intermediate *EMA*, peak MT power output exceeded instantaneous peak CE power (Fig. 6 A). Most strikingly, the inertial load was more than 20-fold greater than the drag load, causing SEE stretch and recoil both to occur within the period of load acceleration before peak drag was reached. During this rapid rise in force, both CE and MT velocity shortened to ~80% V_{max} as the SEE recoiled. The timing of peak elastic recoil velocity coincided with peak CE power, causing MT power enhancement. A similar general pattern was observed for all six simulations where power amplification occurred. As a representative example, the above simulation is shown, but with decreased *EMA* (Fig. 6B). Similarly, inertial loading was ~23-fold greater than drag loading. Immediately following the onset of activation, CE shortening velocity accelerated nearly to 1/3 V_{max}. Unlike the prior case, CE velocity remained close to 1/3V_{max} until the tendon reached peak recoil velocity. Additionally due to the decreased *EMA*, peak MT force increased, causing maximum CE power occurring simultaneously with peak SEE power, hence power amplification.

3.5. Determining the relative influence of mass, β and EMA on MT power output

Among the three parameters varied across simulations, a sensitivity analysis revealed that peak MT power output was most strongly influenced by shifts in *EMA* (Fig. 7). Depending on the values for both β and mass, a slight increase in *EMA* either caused a decrease or an increase in MT power (see Discussion for further details). In addition to *EMA*, increases in mass caused increases in MT power at low masses, but not at high mass values. Further, for most points in the sensitivity analysis, increases in fluid loading (i.e., β) caused MT power to decrease. This suggests that, for many conditions, either *EMA* or mass must shift to accommodate changes in fluid loading to maintain power output. Yet, a notable exception to the inverse relationship between power and β appears at low mass (Fig. 7A) where a 10% increase in β caused a ~5% increase in MT power, explaining the dramatic ~120% increase from $\beta=0.01$ to 0.1 (Fig. 4A) at *EMA*=0.05. In this

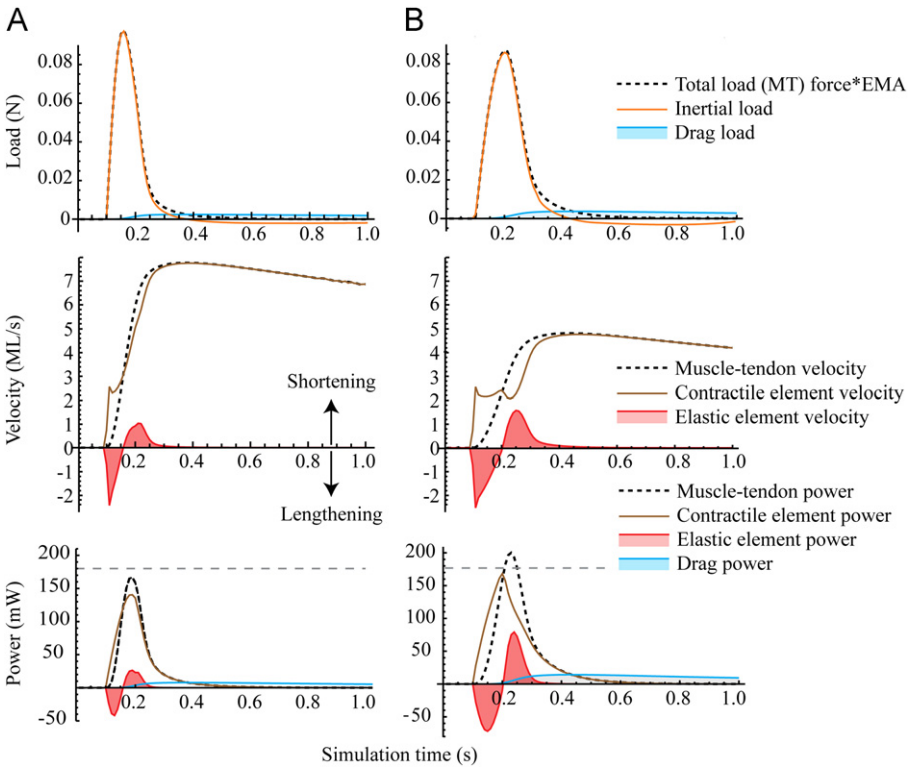

Fig. 6. Data traces from (A) a power enhancing simulation (mass=3 g, $\beta=10^{-3}$, *EMA*=0.05) and (B) a power amplifying simulation (mass=3 g, $\beta=10^{-3}$, *EMA*=0.025). Upper panels show the total (dashed), inertial (orange) and drag (blue, shaded) components of load. Note that because total load=MT force × *EMA*, MT force is higher in (B) because of lower EMA. Middle panels show muscle–tendon (MT; dashed), contractile element (CE; brown) and series elastic element (SEE; red, shaded) components of velocity. Lower panels show muscle–tendon (MT; dashed), contractile element (CE; brown), drag (blue shaded) and series elastic element (SEE; red, shaded) components of power. The dashed grey line represents the CE power limit.

case the increase in fluid loading caused the CE to shorten at $\sim 0.3V_{max}$ during peak muscle activation, vs. $0.6V_{max}$ at lower β.

4. Discussion

4.1. Emergence of power amplification vs. power attenuation depends on effective mechanical advantage and load

Based on realistic frog hind limb morphology and muscle–tendon properties, we implemented a simple mathematical muscle–tendon (MT) model to determine whether elastic recoil enhances or attenuates MT power in water. Previous research has shown evidence for MT power outputs exceeding muscle power limits in jumping frogs (Marsh and John-Alder, 1994; Peplowski and Marsh, 1997; Galantis and Woledge, 2003), particularly when effective mechanical advantage (*EMA*) ≈ 0.1 (Roberts and Marsh, 2003). Yet, since frog hind limbs experience far lower forces in water vs. land (Nauwelaerts and Aerts, 2003; Nauwelaerts et al., 2005), we expected that a compliant tendon at *EMA*=0.1 would not enhance power during swimming. Rather, we expected that elastic recoil in water would require lower *EMA* values (<0.1) in order to increase the effective load on the muscle to enable greater elastic energy storage. Additionally, we also predicted that reduced *EMA* would decrease MT power for inertial loads. Thus, we varied limb morphological and loading environment properties by altering mass (inertial loading), 'drag multiplier' (β; fluid drag loading) and *EMA* to test our hypotheses.

In support of our hypothesis, MT power outputs at *EMA*=0.1 were sub-maximal, except for the highest inertial loads (mass=30 g; Fig. 4). Also as expected, reduced *EMA* (=0.025) diminished MT power for the highest mass conditions. Although a muscle contracting in a terrestrial environment might experience high inertial loads (e.g., to accelerate the 30 g body mass), such high inertial loads are unlikely during swimming. Thus, for comparison, simulations were also performed at a more realistic limb mass for swimming (3 g). Consistent with our hypothesis, power was sub-maximal at *EMA*=0.1, whereas the lowest *EMA* value elicited maximal MT power output (*EMA*=0.025; Fig. 4B). However, despite causing power amplification at low fluid loads (i.e., $\beta<0.1$), reduced *EMA* unexpectedly caused severe power attenuation at the highest fluid loads.

Thus, among the different simulation conditions, all of the three hypothetical power-producing cases emerged: Power transmitting (Fig. 5A), power attenuating (Fig. 5B), power enhancing (Fig. 6A) and power amplifying (Fig. 6B). Although nominal simulation conditions for *Xenopus laevis* swimming (Fig. 4, black box) did not predict power amplification, other simulations did predict power amplification occurring with fluid as well as inertial loads. Notably, however, we found only a modest maximum power amplification of 1.19 compared to a higher value of ~ 1.4 for comparable limbs against purely inertial loads (Galantis and Woledge, 2003). This discrepancy between power amplification ratios of 1.19 and 1.4 could perhaps stem from the inclusion of fluid loading in our model. Regardless, a $\sim 19\%$ increase in peak power (highest mass and *EMA*, lowest β) is modest compared to an $\sim 80\%$ attenuation in power (lowest mass and *EMA*, highest β).

4.2. Neither MT force nor CE power correlate with MT power output

In vivo muscle studies measuring muscle force against fluid dynamic loads have shown that increases in muscle force

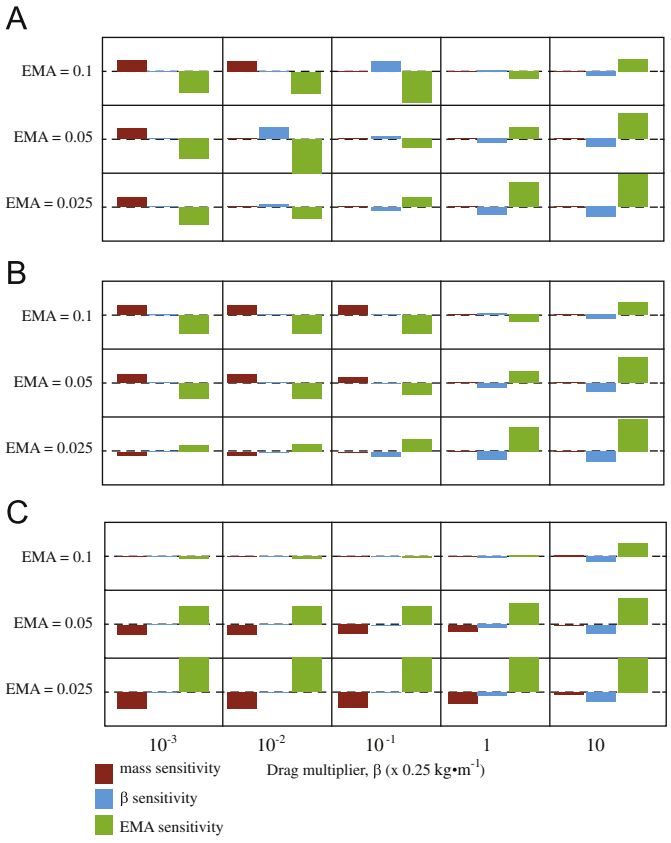

Fig. 7. A sensitivity analysis performed by modulating mass, β, and *EMA* at every point in the parameter space. Bar height represents the magnitude of change in MT peak power output caused by a 10% increase in mass (brown), β (blue) or *EMA* (green). Upward bars represent positive changes whereas downward bars are negative changes. The height of each cell in the grid represents an increase or decrease of 14.2% from the power output value at any given point in the parameter space. Note that for most of the parameter space *EMA* shows the largest bars, therefore exerts the strongest influence on peak MT power output. (A) mass=0.3 g, (B) mass= g and (C) mass=30 g.

correlate to increases in CE power output (Hedrick et al., 2003; Richards and Biewener, 2007). Yet counter to intuition, current simulations do not predict a clear relationship between peak force and peak power output (Fig. 3 vs. Fig. 4). One key distinction is that neural activation-deactivation remains constant in the current model, but is highly variable in vivo. For example, swimming frogs and flying birds increase the number of muscle fibers recruited to increase force and power output (Hedrick et al., 2003; Richards and Biewener, 2007). However, in our model, for a given fixed neural activation-deactivation waveform, the maximum CE power could only vary as a function of shortening velocity. Thus regardless of fluid vs. inertial loading, an increase in load force can either cause an increase or a decrease in CE power, depending on whether shortening velocity is above or below $1/3V_{max}$, respectively. With few exceptions, average CE shortening velocities for the current simulations were higher than $1/3V_{max}$ (measured within $+/-$ 50 ms of peak power), explaining the observed increase in CE power with increasing fluid loading (Fig. 4, second column). Notably however, MT power decreased for greater fluid loads at nearly all points of the sensitivity analysis (Fig. 7), suggesting that despite increasing CE power, some other mechanism is required for power amplification.

An additional implication of the observed trends in peak MT force is that elastic energy storage fails to predict MT power output. Intuitively, peak SEE power correlates positively with the potential energy stored during stretch (Fig. 8A). Yet, this is not the case for MT power. Curiously, simulations storing either very small or very large amounts of elastic energy produced poor MT power outputs. The simulations producing the highest MT power only occurred within a narrow range of 3 to 5 mJ of elastic potential energy (Fig. 8B). However, different simulation conditions (e.g., low mass and low *EMA*) storing a similar amount of work failed to produce power amplification. Unexpectedly, excessive energy storage ($>\sim$8 mJ) was detrimental due to the effects of power attenuation, particularly for large fluid loads and low *EMA* values (Fig. 8B). Thus, current findings suggest that regardless of the nature of the load, both significant amounts of CE power and appropriate energy storage are not sufficient for power amplification without appropriate timing of elastic recoil.

4.3. Variation in loading conditions alters the timing of elastic recoil

Given the importance of both optimal energy storage and CE power, what additional characteristics of MT dynamics are required to confer power amplification? Independent of loading conditions, all power amplifying simulations showed similar temporal patterns of CE and SEE power. Additionally, slightly different conditions were required for maximizing CE power vs. SEE power. For the CE, peak power occurs if activation is at (or near) maximum and if CE shortening velocity is $\sim 1/3V_{max}$. In contrast, the velocity (therefore power) of the SEE is proportional to the rate of force relaxation. If we expect peak force at peak activation, then the maximum rate of force decline and SEE velocity would occur slightly after peak activation where the rate of deactivation is highest. Thus, we expect 'optimal' CE and SEE dynamics to be timed with respect to the timing of peak activation. During ideal loading conditions for generating power (i.e., either high mass or intermediate mass and low *EMA*), the CE reached $\sim 1/3V_{max}$ at 100 ms after excitation onset (=time of peak neural activation) ensuring maximal CE power (Fig. 6B). Independently, the same loading conditions caused tendon stretch and recoil to occur within the first $\sim$200 ms after CE excitation onset, enabling peak recoil power to develop slightly after peak activation and nearly coincide with peak CE power. Specifically, power amplification occurs only if the SEE begins to recoil between 0.18 and 0.2 s (8C) (i.e., 80 to 100 ms after CE excitation onset), slightly after maximum activation. In contrast, simulations in which elastic recoil occurred late ($>\sim$140 ms after stimulation) suffered power attenuation. Thus, for the current model presented, power amplification emerges in this system when three conditions are met: (1) When 3–5 mJ is stored in the SEE prior to recoil, when (2) CE power output is maximum (i.e., shortening at $\sim 1/3V_{max}$) and when (3) elastic recoil occurs within a small window between 0.08 and 0.1 s after excitation onset of the CE.

What properties govern the timing of elastic recoil? As a consequence of the in-series arrangement of the tendon, the timecourse of tendon stretch must follow muscle force (Fig. 2). Thus, the rate-of-change of muscle force governs the timecourse of tendon velocity. Therefore, the tendon *always* begins to recoil at peak MT force (when the rate-of-change of force=0). Consequently, the timing of peak MT force is crucial for determining whether elastic recoil coincides with peak CE power. Importantly, the relative strengths of drag vs. inertial loading influence the observed variation in MT force timing. Because inertial force is proportional to acceleration and drag force to velocity^2, drag force must lag 90° out-of-phase with inertial force. This fundamental property reveals interesting implications for MT dynamics: As the ratio of fluid drag to inertial force increases, peak MT force becomes increasingly delayed. Current simulations suggest that power amplification only occurs if the ratio of inertial force to drag force exceeds 1.5. Otherwise, the timing of elastic recoil is delayed sufficiently beyond 100 ms post muscle excitation,

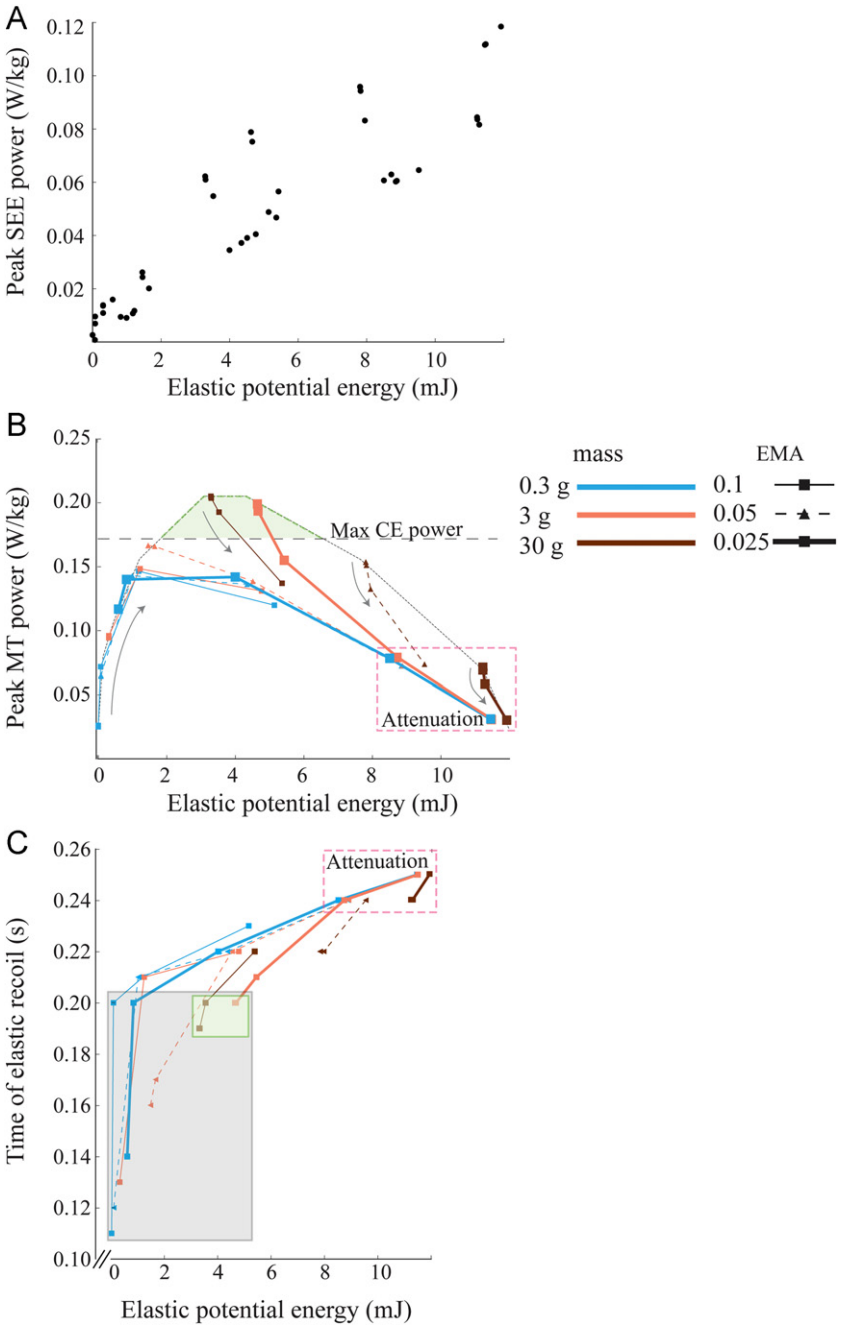

Fig. 8. (A) Peak series elastic element (SEE) power vs. elastic potential energy. (B) Peak muscle–tendon (MT) power output vs. elastic potential energy for mass=0.3 g (blue), mass=3 g (orange) and mass=30 g (brown) each for *EMA*=0.1 (solid lines, squares), *EMA*=0.05 (dashed lines, triangles) and *EMA*=0.025 (thick lines, squares). Horizontal grey-dashed line represents maximum CE power output. Arrows represent increasing β. Note the overall bell-shaped pattern (outlined by the dotted line) representing all simulations with low β values in which inertial loading dominates. The green shaded area represents the area of power amplification. The purple dashed box represents the simulations showing power attenuation. (C) Time of elastic recoil vs. elastic potential energy (same color legend as in B). The grey shaded area represents the area of power enhancement, whereas the green area represents power amplification. The purple dashed box represents the simulations showing power attenuation.

inhibiting the synchronization of maximum CE power and elastic recoil power. Since the tendency for power amplification vs. power attenuation depends on the timing of elastic recoil with neural activation-deactivation, we expect that changes in the neural activation-deactivation pattern (e.g., to represent faster or slower fiber types) will yield different values for optimal energy storage as well as the relative strengths of inertial vs. drag loading. Further modulating the deactivation waveform shape will likely have strong effects on tendon dynamics because tendon recoil velocity is determined by the rate of force decline (hence, the rate of deactivation; Roberts and Marsh, 2003). Additional models are necessary to further generalize the current model's predictions to other vertebrate systems over a range of size and time scales.

4.4. Simplifications of the current model do not diminish its utility

Our simple model was expanded from prior work (Galantis and Woledge, 2003) to include time-dependent activation-deactivation and fluid effects. In the spirit of prior simple models (Alexander, 1997; Curtin et al., 1998; Roberts and Marsh, 2003; Aerts and Nauwelaerts, 2009), the current model captures important aspects

of muscle–tendon–load mechanics in the absence of additional parameters which may obscure the generality of the findings. Despite realistic aspects of the model's morphology and muscle intrinsic properties, a few parameters were omitted. Among these, the most important is the force-length property of muscle fibers (Gordon et al., 1966). Although varying the initial starting length of muscle is likely to enhance power output (Azizi and Roberts, 2010; Clemente and Richards, 2012), the current model kept muscle starting length fixed. As observed in pilot trials, simulations which included force-length properties followed identical trends, but at lower values of peak force and power as the ones presented currently. Therefore, we conclude that muscle force-velocity and activation-deactivation dynamics are the most important properties governing muscle mechanics for the current parameters tested. A second parameter that is potentially important is a time-varying *EMA*. For example, *EMA* may increase as in-lever distance grows during joint extension (Roberts and Marsh, 2003) or through dynamic out-lever changes as the body and limb posture shift during a locomotor stride (Carrier et al., 1994; Carrier et al., 1998). When *EMA* is allowed to vary through time, there is no predicted limit for power amplification (Galantis and Woledge, 2003), implying that extreme cases of power amplification could enable the tendon to far exceed muscle power output. Alternatively, dynamic gearing may improve MT power for a 'poorly tuned' system which might otherwise undergo power attenuation with a static *EMA*. Regardless, given that SEE power requires the rapid relaxation of MT force, the inclusion of history-dependent effects such as shortening deactivation (e.g., Edman, 1975; Josephson and Stokes, 1999) in addition to dynamic *EMA* is expected to further enhance MT power output in future modeling studies. Additionally, changes in SEE stiffness, k, could influence MT dynamics. Yet we found that, repeating the current simulations at additional stiffness values of 1667, 2500 and 5000 only caused small ($\sim$1%) decreases in peak power values observed over the parameter space. However, varying stiffness values may have a stronger effect when coupled with dynamic changes in *EMA*. Finally, the forward motion of the body was not considered in the current study. Rather, the current model resembles the initial kick of a swimming frog which translates its feet backward through still water before the body begins to accelerate late in the stroke (Johansson and Lauder, 2004; Nauwelaerts et al., 2005; Richards, 2010). Although future modifications including forward body translation would increase the model's biological relevance, the added body dynamics are beyond the current aim to understand MT dynamics during fluid loading. Furthermore, a kinematically realistic model would complicate the current findings and potentially obscure the clear relationships between limb properties and MT power output. All of the above modifications along with the current findings build the predictions that will be tested using recently developed experimental tools enabling measurement of in vitro muscle power in the context of real world loads (Sheppard et al. 2009; Richards, 2011; Richards and Clemente, 2012).

4.5. Species diversity of limb kinematics may influence the utilization of elastic recoil

Findings from our simulations bear important implications on frog swimming. Based on studies of frog hind limb kinematics (Gal and Blake, 1988; Nauwelaerts et al., 2005; Richards, 2008; Richards, 2010) the foot can either generate thrust by rotation, translation or both. Furthermore, either motion produces a combination of drag-based (α velocity^2) and added mass-based (α acceleration) thrust (Gal and Blake, 1988; Richards, 2008). Importantly, from the muscle's perspective, added mass-based thrust is identical to an inertial load (i.e., increasing the effective mass of the foot). Incidentally, pipid frogs (e.g., *X. laevis*) rely upon rotational thrust (Richards, 2010). However, among pipids, *Hymenochirus boettgeri* ($\sim$1–2 g body mass) produces mainly added mass-based thrust (Gal and Blake, 1988) whereas *X. laevis* ($\sim$20–30 g) is mostly drag-based (Richards, 2008). We therefore speculate that the loads experienced by the PL in *H. boettgeri* may enable power amplification because the peak added mass/peak drag force ratio (i.e., peak inertial force/drag force) far exceeds our predicted threshold value of 1.5. Additionally, unlike pipid frogs, ranid frogs generate thrust mainly by foot translation (Peters et al., 1996; Johansson and Lauder, 2004; Nauwelaerts et al., 2005). Although the relative contributions of added mass vs. drag-based forces have not yet been modeled for ranid frogs, propulsive force peaks in the first $\sim$20% of the power stroke (Nauwelaerts et al., 2005) when foot acceleration is high. Moreover, translational motion may incur larger acceleration-based thrust (Richards, 2008). We therefore speculate that 'translational' swimmers (e.g., ranids) may be more likely to produce power amplification (potentially due to higher acclerational/drag forces) than 'rotational' swimmers (e.g., pipids) of similar body size and muscle–tendon properties.

4.6. Summary

Simulations from the current study predict that conditions which confer power amplification during inertial loading are suboptimal for fluid loads, and vice versa. In extreme cases, elastic recoil can reduce MT power by $\sim$80%, compared to a maximum amplification of $\sim$19%. The tendency of a MT system to produce power amplification vs. attenuation depends on load: Low fluid loads, large mass and large *EMA* ($=$0.1) promote power amplification whereas the opposite conditions promote attenuation. Regardless of the different 'optimal' combinations of mass, *EMA* and β, power amplification in current simulations occurs through the optimization of three properties: significant elastic energy storage early in the contraction, maximal CE power output, and optimally timed elastic recoil (i.e., if inertial-drag force ratio $\geq \sim$1.5). Specifically, the elastic energy stored must be sufficient to enable considerable elastic recoil power, but not great enough to delay the timing of elastic recoil beyond the point of maximal neural activation. Additionally, if the drag load is high relative to the inertial load, our findings predict that power amplification will not occur (sometimes incurring power attenuation) due to the phase delay of drag force. Broadly, the current model predicts how MT mechanical output can be 'tuned' to influence performance. Given certain MT intrinsic properties, several sets of different parameter values yield similar results, offering an opportunity to optimize MT power even if a particular parameter (e.g., limb mass or *EMA*) must remain fixed. Thus, current findings suggest that limb mass, muscle intrinsic properties (e.g., F_{max}, V_{max}), SEE stiffness and *EMA* represent a suite of musculoskeletal design parameters that may be 'tuned' over the course of natural selection to enhance locomotor performance.

Acknowledgements

This work was funded by the Rowland Junior Fellows Program at Harvard University. We thank Christofer Clemente and Angela Rivera for helpful comments during the preparation of the manuscript as well as the reviewers for their constructive comments.

References

Aerts, P., 1998. Vertical jumping in Galago senegalensis: the quest for an obligate mechanical power amplifier. Philos. Trans. R. Soc. London, Ser. B: Biol. Sci. 353, 1607–1620.

Aerts, P., Nauwelaerts, S., 2009. Environmentally induced mechanical feedback in locomotion: frog performance as a model. J. Theor. Biol. 261, 372–378.
Alexander, R., 1997. Optimum muscle design for oscillatory movements. J. Theor. Biol. 184, 253–259.
Astley, H.C., Roberts, T.J., 2011. Evidence for a vertebrate catapult: elastic energy storage in the plantaris tendon during frog jumping. Biol. Lett..
Azizi, E., Roberts, T.J., 2010. Muscle performance during frog jumping: influence of elasticity on muscle operating lenghts. Proc. R. Soc. London, Ser. B. Biol. Sci. 277, 1523–1530.
Bennet-Clark, H.C., Lucey, E.C.A., 1967. The jump of the flea: a study of the energetics and a model of the mechanism. J. Exp. Biol. 47, 59–76.
Carrier, D., Heglund, N., Earls, K., 1994. Variable gearing during locomotion in the human musculoskeletal system. Science 265, 651–653.
Carrier, D., Gregersen, C., Silverton, N., 1998. Dynamic gearing in running dogs. J. Exp. Biol. 201, 3185–3195.
Clemente, C.J., Richards, C.T., 2012. Determining the influence of muscle operating length on muscle performance during frog swimming using a bio-robotic model. Bioinspiration Biomimetics 7 (036018), 12.
Curtin, N.A., Gardner-Medwin, A.R., Woledge, R.C., 1998. Predictions of the time course of force and power output by dogfish white muscle fibers during brief tetani. J. Exp. Biol. 201, 103–114.
Edman, K., 1975. Mechanical deactivation induced by active shortening in isolated muscle fibres of the frog. J. Physiol. 246, 255–275.
Emerson, S.B., 1978. Allometry and Jumping in frogs: helping the twain to meet. Evolution 32, 551–564.
Gal, J.M., Blake, R.W., 1988. Biomechanics of frog swimming: I. Estimation of the propulsive force generated by *Hymenochirus boettgeri*. J. Exp. Biol. 138, 399–411.
Galantis, A., Woledge, R.C., 2003. The theoretical limits to the power output of a muscle–tendon complex with inertial and gravitational loads. Proc. R. Soc. London, Ser. B: Biol. Sci. 270, 1493.
Gordon, A.M., Huxley, A.F., Julian, F.J., 1966. The variation in isometric tension with sarcomere length in vertebrate muscle fibres. J. Physiol. 184, 170–192.
Gray, P., Mill, P., 1983. The mechanics of the predatory strike of the praying mantid Heirodula membranacea. J. Exp. Biol. 107, 245.
Hedrick, T.L., Tobalske, B.W., Biewener, A.A., 2003. How cockatiels (Nymphicus hollandicus) modulate pectoralis power output across flight speeds 10.1242/jeb.00272. J. Exp. Biol. 206, 1363–1378.
Hill, A.V., 1938. The heat of shortening and the dynamic constants of muscle. Proc. R. Soc. London, Ser. B: Biol. Sci. 126, 136–195.
Hoerner, S.F., 1965. Fluid Dynamic Drag. Published by the author, Midland Park, NJ.
James, R.S., Wilson, R.S., 2008. Explosive jumping: extreme morphological and physiological specializations of Australian rocket frogs (*Litoria nasuta*). Physiol. Biochem. Zool. 81 (2), 176–185.
Johansson, L.C., Lauder, G.V., 2004. Hydrodynamics of surface swimming in leopard frogs (Rana pipiens). J. Exp. Biol. 207, 3945–3958.
Josephson, R., Stokes, D., 1999. Work-dependent deactivation of a crustacean muscle. J. Exp. Biol. 202, 2551–2565.
Lutz, G.J., Rome, L.C., 1994. Built for jumping: the design of the frog muscular system. Science 263, 370–372.
Marsh, R., John-Alder, H., 1994. Jumping performance of hylid frogs measured with high-speed cine film. J. Exp. Biol. 188, 131–141.
Nauwelaerts, S., Aerts, P., 2003. Propulsive impulse as a covarying performance measure in the comparison of the kinematics of swimming and jumping in frogs 10.1242/jeb.00690. J. Exp. Biol. 206, 4341–4435.
Nauwelaerts, S., Stamhuis, E.J., Aerts, P., 2005. Propulsive force calculations in swimming frogs I. A momentum-impulse approach 10.1242/jeb.01509. J. Exp. Biol. 208, 1435–1443.
Otten, E., 1987. A myocybernetic model of the jaw system of the rat. J. Neurosci. Methods 21, 287–302.
Peplowski, M., Marsh, R., 1997. Work and power output in the hindlimb muscles of Cuban tree frogs Osteopilus septentrionalis during jumping. J. Exp. Biol. 200, 2861–2870.
Peters, S.E., Kamel, L.T., Bashor, D.P., 1996. Hopping and swimming in the Leopard Frog, Rana pipiens: I. step cycles and kinematics. J. Morphol. 230, 1–16.
Reilly, S.M., Jorgensen, M.E., 2011. The evolution of jumping in frogs: morphological evidence for the basal anuran locomotor condition and the radiation of locomotor systems in crown group anurans. J. Morphol. 272, 149–188.
Richards, C.T., Biewener, A.A., 2007. Modulation of in vivo muscle power output during swimming in the African clawed frog (*Xenopus laevis*). J. Exp. Biol. 210, 3147–3159.
Richards, C.T., 2008. The kinematic determinants of anuran swimming performance: an inverse and forward dynamics approach. J. Exp. Biol. 211, 3181–3194, http://dx.doi.org/10.1242/jeb.019844.
Richards, C.T., 2010. Kinematics and hydrodynamics analysis of swimming anurans reveals striking inter-specific differences in the mechanism for producing thrust. J. Exp. Biol. 213, 621–634.
Richards, C.T., 2011. Building a robotic link between muscle dynamics and hydrodynamics. J. Exp. Biol. 214, 2381–2389.
Richards, C. T. and Clemente, C. J., 2012. A bio-robotic platform for integrating internal and external mechanics during muscle-powered swimming. Bioinspiration Biomimetics, 7, 016010.
Roberts, T.J., Marsh, R.L., 2003. Probing the limits to muscle-powered accelerations: lessons from jumping bullfrogs 10.1242/jeb.00452. J. Exp. Biol. 206, 2567–2580.
Rome, L.C., Funke, R.P., Alexander, R.M., Lutz, G., Aldridge, H., Scott, F., Freadman, M., 1988. Why animals have different muscle fibre types. Nature 335, 824–827.
Sheppard, P., Sawicki, G. S., Roberts, T.J. (2009). Power augmentation in a compliant muscle–tendon system. 33rd Annual Meeting of American Society of Biomechanics, August 26–29, State College, Pennsylvania.
Shubin, N.H., Jenkins, Jr., F.A., 1994. An early jurassic jumping frog. Nature 377, 49–52.
Zajac, F.E., 1989. Muscle and tendon: properties, models, scaling, and application to biomechanics and motor control. Crit. Rev. Biomed. Eng. 17, 359.